Science of the Total Environment 898 (2023) 165347

Contents lists available at ScienceDirect

Science of the Total Environment

journal homepage: www.elsevier.com/locate/scitotenv

Intrinsic peroxidase-like activity of dissolved black carbon released from biochar

Yi Tan [a], Su Sun [a], Zehui Deng [a], Pedro J.J. Alvarez [b], Xiaolei Qu [a,*]

[a] State Key Laboratory of Pollution Control and Resource Reuse, School of the Environment, Nanjing University, Jiangsu 210023, China
[b] Department of Civil and Environmental Engineering, Rice University, Houston, TX 77005, United States

HIGHLIGHTS

- DBC released from biochar has intrinsic peroxidase-like activity.
- DBC catalyzes H_2O_2 decomposition into hydroxyl radicals.
- Activity increases with temperature with an optimum at pH 5.
- Peroxidase-like activity of DBC follows the ping-pong mechanism.

GRAPHICAL ABSTRACT

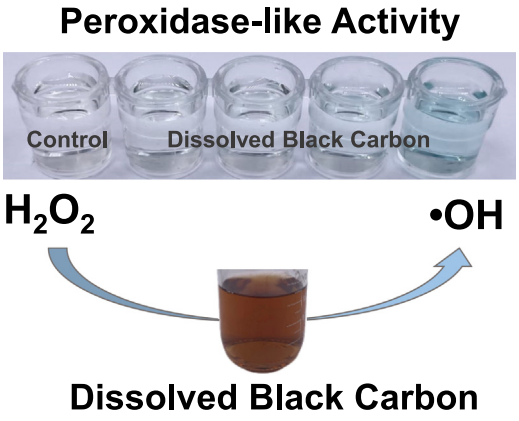

ARTICLE INFO

Editor: Fang Wang

Keywords:
Peroxidase-like activity
Dissolved black carbon
Biochar
Hydrogen peroxide
Hydroxyl radicals

ABSTRACT

Dissolved black carbon (DBC) is an important constituent of the natural organic carbon pool, influencing the global carbon cycling and the fate processes of many pollutants. In this work, we discovered that DBC released from biochar has intrinsic peroxidase-like activity. DBC samples were derived from four biomass stocks, including corn, peanut, rice, and sorghum straws. All DBC samples catalyze H_2O_2 decomposition into hydroxyl radicals, as determined by the electron paramagnetic resonance and the molecular probe. Similar to enzymes that exhibit saturation kinetics, the steady-state reaction rates follow the Michaelis – Menten equation. The peroxidase-like activity of DBC is controlled by the ping-pong mechanism, as suggested by parallel Lineweaver – Burk plots. Its activity increases with temperature from 10 to 80 °C and has an optimum at pH 5. The peroxidase-like activity of DBC is positively correlated with its aromaticity as aromatics can stabilize the reactive intermediates. The active sites in DBC also involve oxygen-containing groups, as inferred by increased activity after the chemical reduction of carbonyls. The peroxidase-like activity of DBC has significant implications for biogeochemical processing of carbon and potential health and ecological impacts of black carbon. It also highlights the need to advance the understanding of the occurrence and role of organic catalysts in natural systems.

1. Introduction

Black carbon (BC) is the recalcitrant carbon residue originating from the incomplete combustion of fossil fuel and biomass, playing a critical role in the global carbon cycle (Masiello, 2004; Woolf et al., 2010). Dissolved black

* Corresponding author.
E-mail address: xiaoleiqu@nju.edu.cn (X. Qu).

http://dx.doi.org/10.1016/j.scitotenv.2023.165347
Received 16 April 2023; Received in revised form 4 July 2023; Accepted 4 July 2023
Available online 5 July 2023

carbon (DBC) is the soluble fraction of the BC continuum. It is a significant part of the riverine dissolved organic carbon pool (~10 %), which comprises the major flux of terrestrial BC to the oceans (Jaffe et al., 2013). DBC is actively involved in the global carbon cycle and the environmental fate of many pollutants (Fu et al., 2016; Fu et al., 2018a). It contains abundant aromatic, aliphatic, and carboxylic structures that enhance its sorptive properties towards pollutants (Fu et al., 2018a; Qu et al., 2016; Song et al., 2021) and is photoactive under solar irradiation, generating reactive phototransients such as triplet-excited state, singlet oxygen ($^1O_2$), and superoxide ($O_2^{\cdot-}$) (Fu et al., 2016; Lian et al., 2021; Wang et al., 2020b). Thus, DBC can serve as an efficient photosensitizer to oxidize pollutants (Fang et al., 2017; Wan et al., 2021; Wang et al., 2022; Zhou et al., 2018). Recent studies reported that BC nanoparticles released from biochar contain persistent free radicals (PFRs) generated during the charring process (Lian et al., 2020; Liu et al., 2020). Such PFRs can induce oxidative stress in rice plants (Liu et al., 2020) and damage environmental DNA, and inhibit the replication of antibiotic resistance genes (Lian et al., 2020). These examples illustrate that BC can mediate important and diverse redox processes in the environment. However, our understanding of the catalytic activity of DBC without light is very limited.

Several carbonaceous nanomaterials exhibit peroxidase-like activity, including carboxylated carbon nanotubes (Song et al., 2010b), carboxyfullerenes (Li et al., 2013), graphene oxides (Song et al., 2010a; Wang et al., 2020a), graphene quantum dots (Sun et al., 2014; Sun et al., 2015; Zheng et al., 2013), and carbon quantum dots (Shi et al., 2011). They can catalyze the oxidation of peroxidase substrates such as 3,3,5,5-tetramethylbenzidine (TMB) with H_2O_2, similar to natural peroxidases (*e.g.*, horseradish peroxidase, HRP). The peroxidase-like activity of carboxylated single-walled carbon nanotubes and graphene oxides has been exploited for analytical purposes (Song et al., 2010a; Song et al., 2010b; Wang et al., 2020a). Similarly, graphene quantum dots and carbon quantum dots have a peroxidase-like activity that has been proposed for glutathione (Sun et al., 2014; Sun et al., 2015; Zheng et al., 2013) and glucose detection (Shi et al., 2011), respectively. The peroxidase-like activity of graphene oxides is apparently related to its oxygen-containing and aromatic groups (Song et al., 2010a; Sun et al., 2014; Sun et al., 2015; Wang et al., 2020a; Zhao et al., 2015). Specifically, the larger aromatic cluster was reported to confer higher peroxidase-like activity by stabilizing the reactive intermediates (Zhao et al., 2015). Also, carbonyl groups were found to be responsible for the enzyme-like activity, while the carboxyl groups were the major binding sites (Sun et al., 2015; Wang et al., 2020a). In contrast, hydroxyl groups were found to hinder the peroxidase-like activity by trapping •OH (Sun et al., 2015).

DBC is a continuum of macromolecules (Xu et al., 2017), drastically different from these aforementioned carbonaceous nanomaterials with crystalline carbon structures. Currently, little is known about the enzyme-mimic activity of environmentally occurring amorphous carbon materials. DBC contains both aromatic and oxygen-containing groups (Qu et al., 2016). We hypothesize that DBC released from biochar has significant (and so far overlooked) peroxidase-like activity. If so, it is important to determine whether this activity is intrinsic, because H_2O_2 is ubiquitous in aquatic systems, including surface water (0– 180 ppb) (Ndungu et al., 2019), groundwater (0.2– 1.3 ppb) (Yuan et al., 2017), rainwater (119– 2414 ppb) (Shaked et al., 2010; Yuan and Shiller, 2000), cloud water (0– 639 ppb) (Marinoni et al., 2011), seawater (0.3– 3.1 ppb) (Shaked et al., 2010), and even geothermal water (6.8– 20.4 ppb) (Wilson et al., 2000), partly due to photochemical reactions, with concentrations commonly reaching the ppb – ppm range. H_2O_2 also can be generated under dark conditions through biological processes, redox cycling of metals, and interactions between metal and reduced organic matter (Page et al., 2012; Yuan et al., 2017). Thus, the peroxidase-like activity of DBC, catalyzing H_2O_2 decomposition into hydroxyl radicals, would have significant implications on the carbon cycle, the fate processes of pollutants, and the potential environmental health impacts of black carbon.

In this study, we evaluated the peroxidase-like activity of DBC samples derived from four biomass stocks, using TMB as colorimetric probe. The generation of reactive oxygen species (ROS) during the catalytic reactions was determined by electron paramagnetic resonance (EPR) and molecular probes. Whether reaction rates followed saturation kinetics was investigated using the Michaelis-Menten equation and Lineweaver-Burk linearization plots. The potential role of aromatic and carbonyl groups in the peroxidase-like activity of DBC was examined. To the best of our knowledge, this is the first report of the significant peroxidase-like activity of environmentally occurring amorphous carbon materials.

2. Materials and methods

2.1. Materials

Hydrogen peroxide (H_2O_2, 30 %) was obtained from Nanjing Chemical Reagent Co., Ltd., China. 3,3,5,5-tetramethylbenzidine (TMB, 99 %), terephthalic acid (TPA, 98 %), 2-hydroxyterephthalic acid (*h*TPA, 98 %), furfuryl alcohol (FFA, 98 %), 2,3-bis(2-methoxy4-nitro-5-sulfophenyl)-2H-tetrazolium-5-carboxanilide (XTT, > 90 %), 5,5-Dimethyle-1-pyrolene N-oxide (DMPO, 98 %), 2,2,6,6-tetramethyl-4-piperidinol (TEMP, 98 %), sodium borohydride ($NaBH_4$, >98 %), and deionized water (18.2 MΩ·cm resistivity at 25 °C) was used in this study.

2.2. Preparation and reduction of DBC

DBC was made from the water extracts of biochar derived from corn, peanut, rice, and sorghum straws and underwent demineralization as described in the literature (Fu et al., 2016; Fu et al., 2018b). Biochar samples were synthesized by pyrolyzing pulverized biomass in the muffle furnace. The temperature was set to increase from 20 to 400 °C at a rate of 5 °C/min and held for 3 h. The biochar was then grounded and sieved (100-mesh). Fifty grams of biochar were dispersed in 800 mL deionized water by stirring and sonicated for 30 min at 100 W in a bath sonicator. The suspension was filtered by 0.45-μm membranes (ANPEL Laboratory Technologies Shanghai Inc., China). The residue on the membranes went through another round of water extraction. The extraction process was repeated three times. All the collected solution was freeze-dried. One gram of the resulting powder was demineralized in 10 mL of 1 M HCl and 1 M HF solution for 4 h. After neutralizing with NaOH, the DBC solution was dialyzed with a dialysis membrane (MWCO 1000 Da, VAKE, USA) against deionized water. The resulting sample was freeze-dried and referred to as DBC.

$NaBH_4$ was used to selectively reduce the carbonyl groups using a procedure modified from previous studies (McKay et al., 2016; Sharpless, 2012). Forty milliliters DBC (50 mgC/L) was bubbled with N_2 for 30 min to remove the dissolved oxygen. A 10-fold excess $NaBH_4$ was then added during the stirring at 200 rpm. N_2 was continuously sparged into the mixture for 3 h. The HCl solution was added to the solution until pH 5.0 and then the air was sparged into the solution for 1 h to quench the residual $NaBH_4$. The solution was dialyzed with a dialysis membrane (MWCO 100 Da, VAKE, USA) against deionized water for 48 h and freeze-dried.

2.3. Characterization of DBC

DBC samples were subjected to transmission electron microscopy (TEM), scanning electron microscopy (SEM), Raman, Fourier-transform infrared spectroscopy (FT-IR), X-ray photoelectron spectroscopy (XPS), and proton nuclear magnetic resonance (^{1}H NMR) analysis. Details of the analysis were summarized in Supplementary Data Text S1.

2.4. Measurement of the peroxidase-like activity of DBC

The peroxidase-like activity of DBC was examined by the catalytic oxidation of TMB with H_2O_2. Typically, 400 μL DBC solution (15 mgC/L) was mixed with 510 μL acetate buffer (pH 5.0, 0.2 M), ten μL TMB (10 mM in DMSO), and 80 μL H_2O_2 (0.1 M). If DBC possesses peroxidase-like activity, it can activate H_2O_2 and oxidize the colorless TMB to its oxidized state (oxTMB) with a characteristic absorbance at

652 nm. The absorbance at 652 nm of the system was monitored using a UV-2700 spectrophotometer (SHIMADZU, Japan). The influence of temperature and pH on the activity of DBC was examined by changing the pH (pH 2–9) or temperature (10–80 °C) of the reaction system.

The steady-state kinetics of the catalytic reaction was investigated to assess the activity of DBC. The initial velocity (V) at different concentrations of H_2O_2 and TMB was measured by the change of absorbance at 652 nm. V values were then used to calculate the enzymic kinetic parameters, including Michaelis–Menten constant (K_m) and maximum catalytic velocity (V_{max}) based on the Michaelis-Menten equation (Eq. (1)):

$$V = \frac{V_{max}[S]}{V_m + [S]} \tag{1}$$

where [S] is the concentration of the substrate (TMB or H_2O_2 in this study).

The peroxidase-like activity assay was carried out by varying the concentrations of TMB or H_2O_2 while keeping the other constant at three different concentrations to further explore the kinetic mechanism of the catalytic reaction. The kinetic data were plotted in the Lineweaver–Burk form (Eq. (2)). There are two major kinetic mechanisms in bi-substrate enzyme reactions: the ping-pong mechanism (double replacement reaction) and the sequential mechanism (ternary complex formation). If the Lineweaver-Burk plots of substrates at different concentrations are parallel, the reaction is controlled by the ping-pong mechanism. Otherwise, the reaction is controlled by the sequential mechanism.

$$\frac{1}{V} = \frac{K_m}{V_{max}} \times \frac{1}{[S]} + \frac{1}{V_{max}} \tag{2}$$

The initial velocity equation of the bi-substrate reaction can be expressed in the Dalziel's form (Eq. (3)) and further transformed into Eq. (4).

$$\frac{[E]}{V} = \theta_0 + \frac{\theta_1}{[TMB]} + \frac{\theta_2}{[H_2O_2]} + \frac{\theta_{12}}{[TMB][H_2O_2]} \tag{3}$$

$$\begin{aligned}\frac{[E]}{V} &= \left(\theta_0 + \frac{\theta_1}{[TMB]}\right) + \left(\theta_2 + \frac{\theta_{12}}{[TMB]}\right) \times \frac{1}{[H_2O_2]} \\ &= \left(\theta_0 + \frac{\theta_2}{[H_2O_2]}\right) + \left(\theta_1 + \frac{\theta_{12}}{[H_2O_2]}\right) \times \frac{1}{[TMB]}\end{aligned} \tag{4}$$

Where [E] is the DBC molar concentration calculated using the molecular weight of DBC, which was determined to be 3600 Da in the previous study (Zhou et al., 2018), V is the initial velocity, [TMB] and [H_2O_2] are the concentrations of the substrates, θ_1 and θ_2 are the Dalziel coefficients associated with TMB and H_2O_2 respectively, and θ_{12} is the Dalziel coefficient associated with both substrates. The value of θ_{12} is determined by the slope value of a linear fitting of the slope values from the Lineweaver-Burk plots ($\theta_1 + \theta_{12}/[H_2O_2]$) in Fig. 5b against $1/[H_2O_2]$.

2.5. Measurements of reactive oxygen species (ROS)

The production of ROS during the reaction was examined by molecular probes. $^1O_2$, O_2^- and •OH were probed using FFA (Haag et al., 1984), XTT (Ishibashi et al., 2000; Sutherland and Learmonth, 1997), and TPA (Ishibashi et al., 2000), respectively. For most experiments, 15 mgC/L DBC was mixed with probe molecule solutions and 100 mM H_2O_2 in a 50 mL glass beaker under dark conditions. The solution was periodically sampled to analyze the probe molecule. Solutions without DBC were used as controls. The generation of $^1O_2$ was measured by observing the reduction in the concentration of FFA as described previously (Haag et al., 1984). FFA was measured using an HPLC equipped with a Zorbax Eclipse XDB-C18 column (Agilent 1100, Agilent Technologies, USA) at 220 nm with 30 % acetonitrile and 70 % 0.1 wt% phosphoric acid as the mobile phase. The formation of XTT formazan was used to measure the generation of O_2^- (Chen and Jafvert, 2011; Sutherland and Learmonth, 1997). XTT formazan concentration was quantified at 470 nm using a UV–vis spectrophotometer (UV-2700, SHIMADZU, Japan). The formation of *h*TPA from the oxidation of TPA was used to measure •OH. *h*TPA was quantified by the fluorescence intensity recorded at an excitation wavelength of 315 nm and an emission wavelength of 425 nm on a Horiba Aqualog fluorometer (HORIBA, Japan). The measurements were carried out in triplicate.

EPR was also employed to probe the formation of ROS. The EPR spectra were acquired on an EMXmicro-6/1spectrometer (Bruker, Germany) with an attenuation of 20 dB (0.2 mW microwave power) and 1G modulation amplitude. The spin trapping agent DMPO was employed to probe the formation of •OH in the aqueous solution and the formation of O_2^- in methanol. TEMP was used for the detection of $^1O_2$. Solutions without DBC were used as controls.

3. Results and discussion

3.1. Characterization of dissolved black carbon

DBC samples were released from biochar originating from corn, peanut, sorghum, and rice biomass stocks and demineralized. They formed brown homogeneous solutions in water. The TEM and SEM micrographs of DBC show gel-like aggregates with no clear crystalline structure (Fig. 1a and b), similar to natural organic matter (Wilkinson et al., 1999). This is consistent with the literature that DBC is mainly comprised of amorphous carbons with macromolecular structure (Xu et al., 2017), significantly different from previously studied carbonaceous nanomaterials with crystalline carbon structure (*e.g.*, carbon dots, carbon nanotubes, and graphene oxides). The Raman spectra of DBC samples are summarized in Fig. 1c. DBC samples have peaks at 1582 cm^{-1} (G band) and 1350 cm^{-1} (D band). The intensity ratio of D band to G band (I_D/I_G) for DBC, which is reversely related to the in-plane carbon cluster size (Cançado et al., 2006), varies from 0.79 to 0.96, indicating small aromatic carbon cluster sizes. The functional groups of DBC were examined using the FT-IR spectra (Fig. 1d and Fig. S1). The attribution of the FT-IR peaks is summarized in Table S1. The peaks at ~1250 and 1385 cm^{-1} represent the C—O stretching of phenols and CH bending of aldehyde. The intense peak around 1585 cm^{-1} represents the C═O stretching of conjugated ketones or aromatic C═C stretching. The peaks at ~1710 and 2600 cm^{-1} are linked to the C═O stretching and OH stretching of carboxyls, respectively. The broad peak at ~3400 cm^{-1} represents the OH stretching of H-bonded hydroxyl groups. Thus, DBC macromolecules have rich oxygen-containing functional groups such as carboxyls, phenols, aldehydes, ketones, and hydroxyls. This conclusion is further supported by the XPS data. The O/C values for corn DBC (CDBC), peanut DBC (PDBC), sorghum DBC (SDBC), and rice DBC (RDBC) as determined by XPS are 0.49, 0.44, 0.45, and 0.49, respectively. The deconvolution of the XPS C(1 s) spectrum of CDBC suggests abundant mono-oxygenated and di-oxygenated carbons (Fig. 1e). The percentages of different protons in DBC from the ^1H NMR analysis were summarized in Fig. 1f and Table S2. The NMR spectra were dominated by the aliphatic protons. The aromatic protons in DBC follows the order of CDBC > PDBC > SDBC > RDBC. These characterization data suggest that DBC contains macromolecules with small aromatic carbon structures substituted by abundant oxygen-containing functional groups, generally consistent with previous characterization studies of DBC (Du et al., 2018; Qu et al., 2016).

3.2. Dissolved black carbon catalyzes the oxidation of peroxidase substrates

The peroxidase-like activity of DBC was assessed by the oxidation of TMB, a commonly used colorimetric probe for peroxidase enzyme activity (Gao et al., 2007). Materials with peroxidase-like activity can activate H_2O_2 and subsequently oxidize the colorless TMB to its blue oxidized state (oxTMB) (Fig. 2a). The addition of 6 mgC/L DBC to the TMB and H_2O_2 mixture induced significant color change (Fig. 2b), while there was little color change after mixing TMB with H_2O_2 without DBC (Fig. 2b, control sample). The UV–Vis spectra of the mixture with DBC samples show absorbance at 652 nm after the reaction, which is the characteristic peak for oxTMB (Fig. 2c). The reaction kinetics was then monitored using the

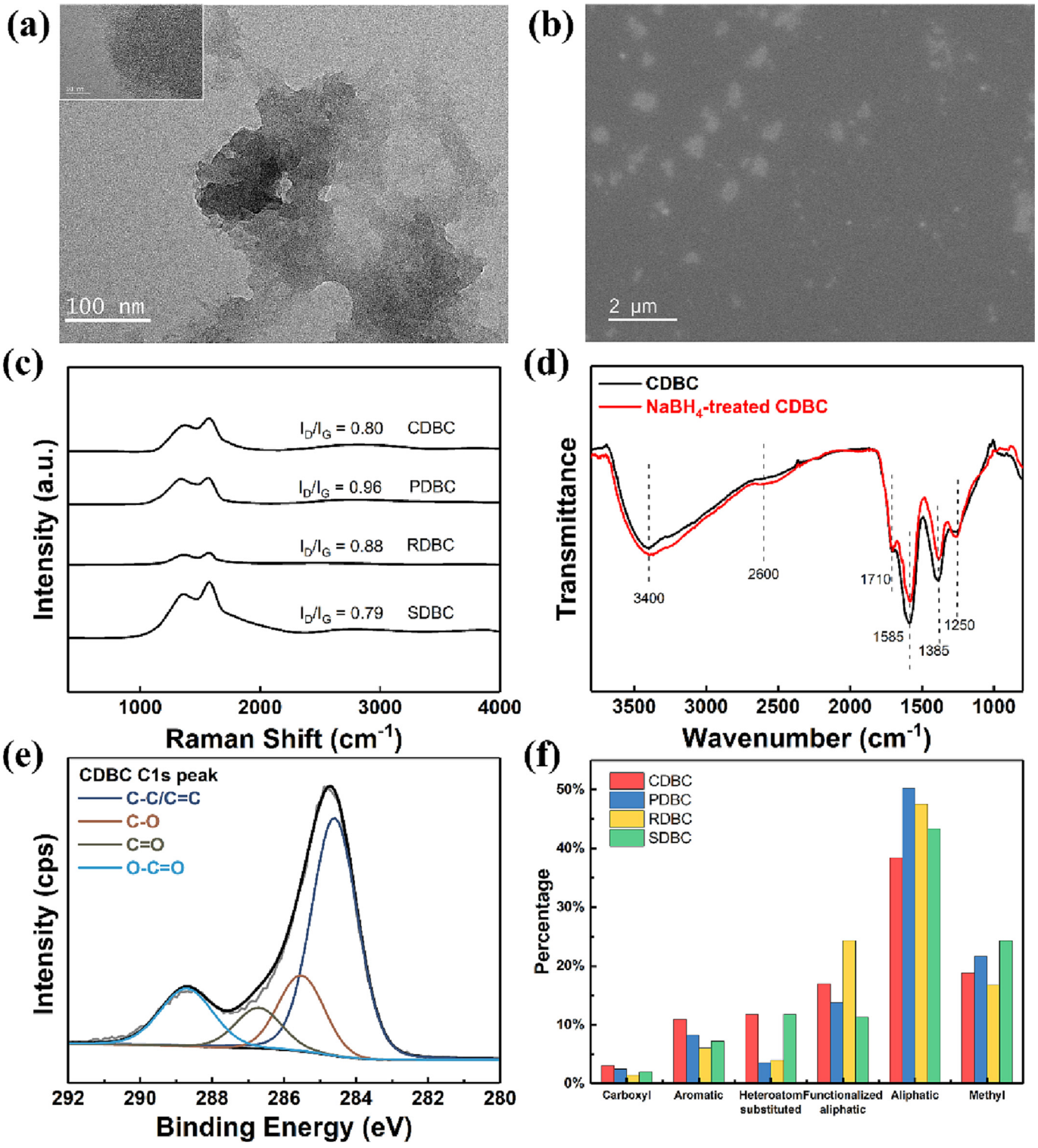

Fig. 1. (a) TEM and (b) SEM micrographs of corn dissolved black carbon (CDBC); (c) Raman spectra of CDBC, peanut DBC (PDBC), sorghum DBC (SDBC), and rice DBC (RDBC); (d) FT-IR spectra of CDBC and $NaBH_4$-treated CDBC; (e) the deconvolution of XPS C(1s) peak of CDBC; (f) the percentages of different protons in DBC as determined by ^1H NMR.

absorbance at 652 nm (Fig. 2d). The formation of oxTMB increased over time for all DBC samples. These results suggest that DBC from different biomass origins all have peroxidase-like activity, following the order: CDBC > PDBC > SDBC, RDBC (Fig. 2c and d). CDBC with the highest peroxidase-like activity was thus used in the majority of the following experiments. It is worth noting that the peroxidase-like activity of DBC can be observed at 0.01 mM H_2O_2, which is an environmentally relevant concentration (Fig. S2).

Peroxidase-mimicking materials often induce free radical generation (*e.g.*, •OH) by H_2O_2 activation (Fan et al., 2018; Lou et al., 2019). ROS generation during the reaction between CDBC and H_2O_2 was examined using molecular probes and EPR (Fig. 2). TPA was used to examine the generation

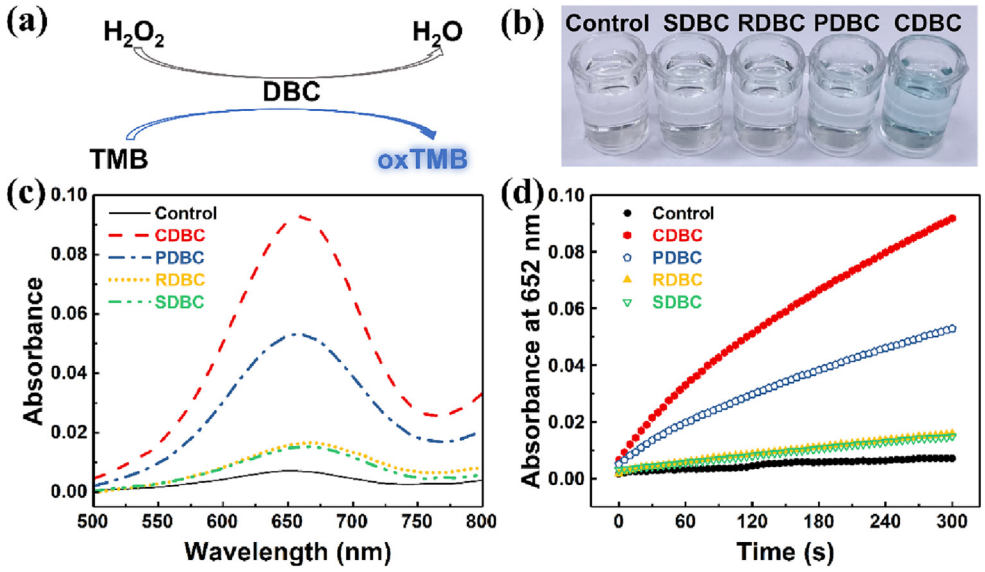

Fig. 2. (a) Schematic illustration of dissolved black carbon (DBC)-mediated TMB oxidation with H_2O_2; (b) photos and (c) UV − vis absorption spectra of mixtures containing 6 mg/L DBC, 0.1 mM TMB and 8 mM H_2O_2 at pH 5.0; (d) The reaction kinetics of DBC-mediated TMB oxidation as reflected by the change of oxTMB absorbance at 652 nm. corn DBC (CDBC), peanut DBC (PDBC), sorghum DBC (SDBC), rice DBC (RDBC).

of •OH (Page et al., 2010). The reaction between TPA and •OH yields fluorescent *h*TPA, whose concentration increased over time in the presence of CDBC and H_2O_2, indicating •OH production (Fig. 3a). The formation of •OH was corroborated by EPR using DMPO as the spin-trapping agent. The EPR spectrum of the mixture of CDBC and H_2O_2 shows a characteristic fingerprint of the DMPO/•OH (a 1:2:2:1 quartet with $a_N = a_H = 14.9$ G), confirming •OH formation (Fig. 3b). There was no significant formation of O_2^- or $^1O_2$ as suggested by EPR analysis (Fig. S4) (Fu et al., 2016). •OH generated by H_2O_2 activation on CDBC is expected to oxidize TMB, yielding blue oxTMB.

The relative activity of CDBC exhibited a nonmonotonic trend with solution pH in the range of pH 2 to pH 9 (Fig. 4a). It increased from pH 2 to pH 5 owing to the stronger interactions between CDBC and TMB as CDBC became more negatively charged with increasing pH (Chen et al., 2018; Fu et al., 2018a). It then significantly decreased at pH > 5 partly due to the decomposition of H_2O_2 (Han et al., 2015). The maximum relative activity occurred at pH around 5, which is generally consistent with the optimum pH for HRP and nanozymes with peroxidase activity (Gao et al., 2007; Jian et al., 2022). The effect of temperature on the catalytic activity of CDBC was also examined. The catalytic activity of CDBC increased with increasing temperature over a range of 10–80 °C (Fig. 4b), similar to luminescent carbon nanoparticles (Wang et al., 2011) and N-doped carbon quantum dots (Lou et al., 2019). This was attributed to the increased thermal motion of the substrate molecules with increasing temperature (Wang et al., 2011). It also suggests the good thermal stability of CDBC.

3.3. The peroxidase-like activity of DBC follows saturation kinetics

The steady-state kinetics of TMB oxidation mediated by H_2O_2 activation by DBC was investigated to gain insight into the catalytic mechanisms. The steady-state kinetics of TMB oxidation was first examined at a fixed H_2O_2 concentration (Fig. 4a). The initial velocity of TMB oxidation (V) increased with the initial TMB concentration ([TMB]) at an H_2O_2 concentration of 9 mM. The correlation between V and [TMB] can be well fitted with the Michaelis-Menten equation ($R^2 = 0.997$, Fig. 5a), which is used to describe the steady-state kinetics of HRP or nanozymes (Gao et al., 2007). Similarly, at a fixed TMB concentration of 0.1 mM, the steady-state kinetics of TMB oxidation at varying H_2O_2 concentrations is well described by the Michaelis-Menten equation ($R^2 = 0.997$, Fig. 5b). Thus, TMB oxidation after H_2O_2 activation by DBC follows saturation kinetics similar to enzymes.

Bi-substrate enzyme reactions are usually controlled by two major catalytic mechanisms: the ping-pong and the sequential mechanisms (Jian et al., 2022). In the ping-pong mechanism, one substrate first reacts with the catalyst to form the intermediate and release a product, then the intermediate reacts with another substrate. The sequential mechanism suggests

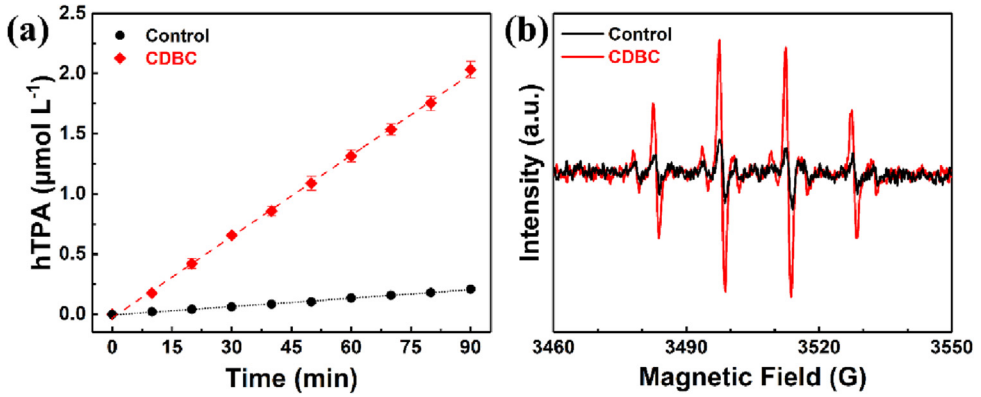

Fig. 3. (a) •OH generation (indicated by *h*TPA formation) increased with reaction time in a mixture of corn dissolved black carbon (CDBC) and H_2O_2. (b) EPR spectrum DMPO adducts confirm generation of •OH in the mixture of CDBC and H_2O_2. Error bars represent ± one standard deviation from the mean of triplicate measurements.

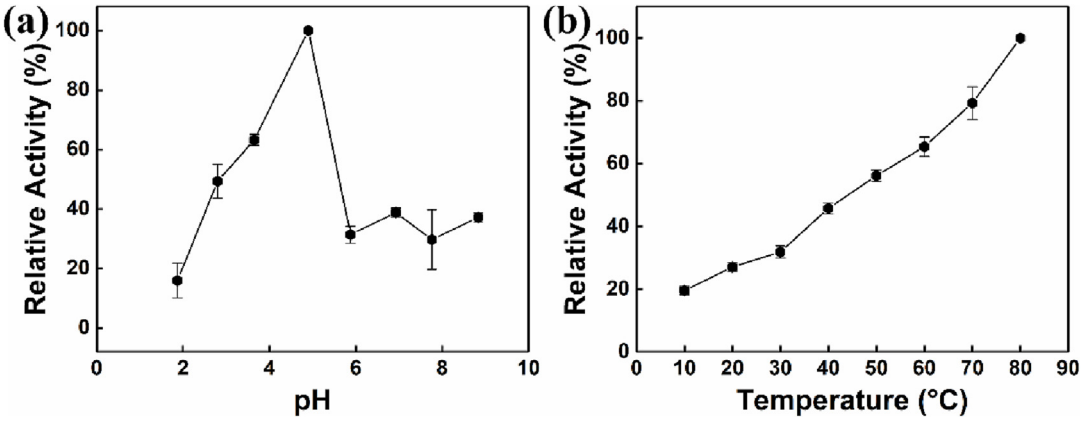

Fig. 4. The peroxidases-like activity of corn dissolved black carbon as a function of (a) solution pH and (b) temperature. Error bars represent ± one standard deviation from the mean of triplicate measurements.

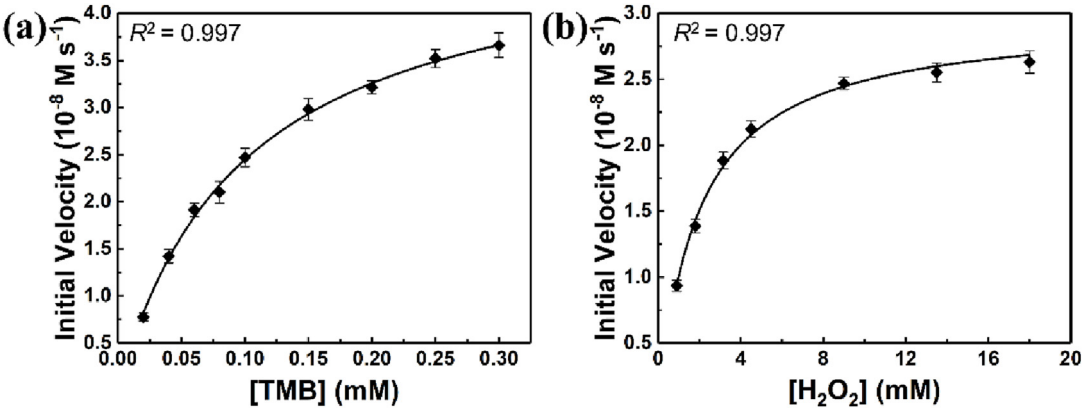

Fig. 5. Peroxidase-like activity of dissolved black carbon (DBC) follows saturation kinetics. (a) The initial velocity of the reaction (V) as a function of the TMB concentration measured with 6 mgC/L corn DBC (CDBC) and 9 mM H_2O_2 at pH = 5; (b) The initial velocity of the reaction (v) as a function of the H_2O_2 concentration measured with 6 mgC/L CDBC and 0.1 mM TMB at pH 5. Error bars represent ± one standard deviation from the mean of triplicate measurements.

that the two substrates bind to the catalyst in a specific order for the reaction to occur. The initial velocity equation of this bi-substrate reaction was expressed in the Dalziel's form (Eqs. (3) and (4)). A high Dalziel coefficient (θ_{12}) suggests the sequential mechanism, while a low θ_{12} value indicates the ping-pong mechanism (Jian et al., 2022). The calculated θ_{12} for CDBC was 0.0053, indicating the dominant role of the ping-pong mechanism. This infers that H_2O_2 was first activated by DBC to generate an intermediate, which in turn oxidizes TMB to oxTMB as indicated by the color change. To further explore the mechanisms for H_2O_2 activation by DBC, Lineweaver – Burk plots were constructed at three different TMB and H_2O_2 concentrations (Fig. 6). The Lineweaver – Burk plots obtained from each fixed substrate dosage are parallel to each other, which is the hallmark pattern for the ping-pong mechanism (Jian et al., 2022).

In order to quantitatively assess the activity of DBC, we calculated their maximum initial velocity (V_{max}) and Michaelis – Menten constant (K_m) based on the kinetic data (Figs. 4, 7, S4, and S6). Michaelis – Menten

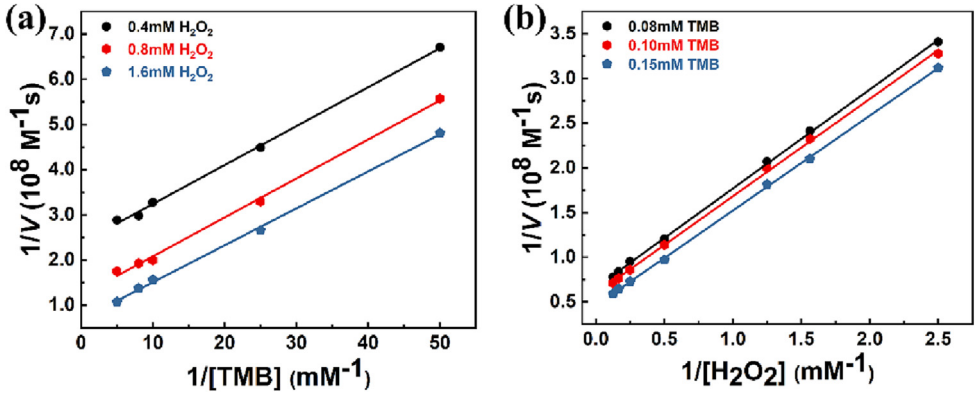

Fig. 6. Ping-pong catalytic mechanism, indicated by parallel Lineweaver – Burk plots of corn dissolved black carbon (CDBC) with varying (a) TMB with three different H_2O_2 dosages; and (b) H_2O_2 with three different TMB dosages.

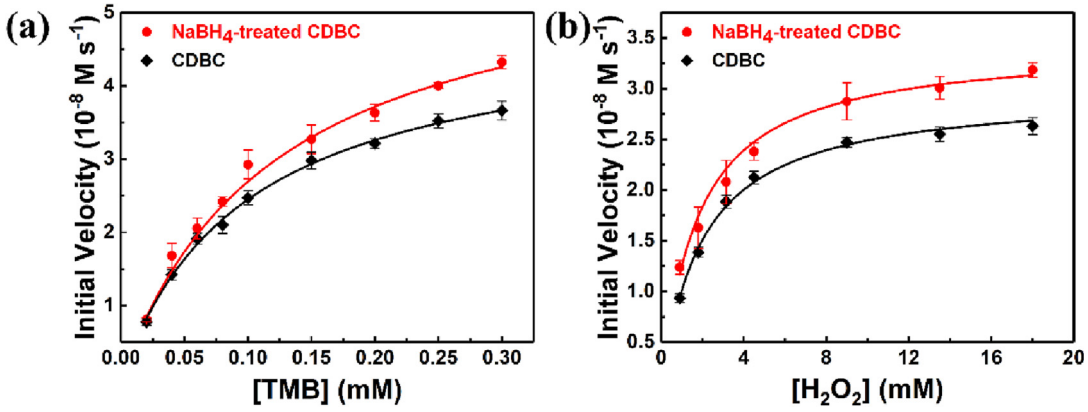

Fig. 7. Increased peroxidase-like activity of corn dissolved black carbon (CDBC) after reduction of carbonyl groups with $NaBH_4$.

parameters for different DBC sources are summarized in Table 1. The K_m values represent the affinity of substrates with enzymes (Gao et al., 2007; Jian et al., 2022). Substrates with high affinity for an enzyme have relatively low K_m values. The K_m values of the tested DBC for H_2O_2 ranged from 0.67 to 2.01 mM, which is lower than that of HRP (3.70 mM). Similarly, K_m values of DBC for TMB ranged from 0.10 to 0.48 mM, also lower than that of HRP (0.43 mM). Thus, DBC has a stronger affinity towards H_2O_2 and TMB than HRP. Among the tested DBC samples, CDBC had the lowest K_m value for TMB, indicating its high affinity towards TMB. The V_{max}/K_m ratio can be used to quantify the catalytic efficiency of enzymes and nanozymes (Gao et al., 2007; Jian et al., 2022). The V_{max}/K_m values of DBC for TMB were in the range of 2.92– 48.70 $\times$ 10^{-5} s^{-1}, with the highest value corresponding to CDBC.

Previous studies of graphene oxides suggest that the aromatic and carbonyl groups are likely the active sites for their peroxidase-like activity (Song et al., 2010a; Sun et al., 2014; Sun et al., 2015; Wang et al., 2020a; Zhao et al., 2015). The relationships between DBC peroxidase-like activity and the abundance of functional groups were examined using ^{1}H NMR data (Fig. 1f and Table S2). There is a significant positive correlation between the aromatic protons of DBC and its peroxidase-like activity (p = 0.029, Fig. S5). The aromatic structure of DBC is expected to facilitate its peroxidase-like activity by stabilizing the reactive intermediates (Zhao et al., 2015). The carbonyl groups of dissolved organic matter (DOM) can be selectively reduced by $NaBH_4$ to form alcohols, phenols, and hydroquinones (Ma et al., 2010; McKay et al., 2016; Tinnacher and Honeyman, 2007). In this work, CDBC was reduced with $NaBH_4$ to remove carbonyl groups and accordingly assess their potential role in the observed peroxidase-like activity. The functional groups of CDBC and the $NaBH_4$-treated CDBC were examined using the FT-IR spectra (Fig. 1d). $NaBH_4$-treated CDBC contains less C=O of conjugated ketones than the original sample as suggested by its weaker absorbance at ~1585 cm^{-1}. The absorbance at ~1385 cm^{-1}, which represents the CH bending of aldehydes, also decreased after reduction with $NaBH_4$. On the other hand, absorbance at ~1250 increased after the reduction, indicating the generation of phenols. The broad absorbance at ~3400 cm^{-1}, which represents the OH stretching of H-bonded hydroxyl groups often found in hydroquinones (Aitipamula et al., 2011; Chen et al., 2015), also increased after the reduction. These results suggested that reactions with $NaBH_4$ preferentially reduce carbonyl groups in CDBC to phenols and hydroquinones, similar to the reactions between $NaBH_4$ and DOM (Fu et al., 2016; Ma et al., 2010; Tinnacher and Honeyman, 2007).

The peroxidase-like activity of CDBC increased after the removal of carbonyl groups upon reduction with $NaBH_4$ (Fig. 7 and Table S3). Similar results were achieved with PDBC (Figs. S6 and S7). Thus, unlike graphene oxides, carbonyl groups are most likely not the key active sites for the peroxidase-like activity of DBC. A previous study suggested that hydroquinones in humic substances can reduce H_2O_2 to form •OH (Page et al., 2012). This indicates that the enhanced peroxidase-like activity of DBC after reduction with $NaBH_4$ could be attributed to the formation of hydroquinones from the reduction of carbonyls (Page et al., 2012).

Table 1
Michaelis-Menten parameters of DBC.

Sample	Substrate	V_{max} ($\times 10^{-8}$ M s^{-1})	K_m (mM)	V_{max}/K_m ($\times 10^{-5}$ s^{-1})
CDBC	H_2O_2	2.97	1.94	1.53
	TMB	4.87	0.10	48.70
PDBC	H_2O_2	1.15	2.01	0.57
	TMB	1.69	0.12	14.08
RDBC	H_2O_2	0.22	0.86	0.26
	TMB	1.30	0.34	3.82
SDBC	H_2O_2	0.24	0.67	0.36
	TMB	1.40	0.48	2.92

4. Conclusions

In this study, we discovered that DBC released from biochar has peroxidase-like activity and catalyzes H_2O_2 decomposition into •OH. The steady-state reaction rates follow the Michaelis – Menten equation, similar to natural enzymes. The peroxidase-like activity of DBC is a bi-substrate enzyme reaction controlled by the ping-pong mechanism. It increases with temperature with an optimum at pH 5. The active sites in DBC are not carbonyls but likely involve aromatic structures and hydroquinones. Considering the ubiquitous presence of H_2O_2 in aquatic systems, the significant peroxidase-like activity of DBC represents a previously overlooked natural formation pathway of •OH that may proceed even under dark conditions. The reaction between •OH and dissolved organic carbon, including DBC itself, would lead to degradation and mineralization reactions influencing carbon cycling (Fu et al., 2018b; Goldstone et al., 2002). It is well-known that the degradation of organic pollutants in the environment can be catalyzed by enzymes such as peroxidases and laccases (Bilal et al., 2018). Similarly, DBC could serve as a catalyst to mediate the oxidation of co-occurring pollutants under dark conditions, affecting their environmental fate processes and associated risks. The literature has reported that graphene quantum dots with peroxidase-like activity possess antibacterial properties (Sun et al., 2014). DBC may indirectly stress microorganisms and algae in aquatic systems, which needs further investigation. An improved understanding of the peroxidase-like activity of DBC is also expected to help decipher the potential environmental health impacts of black carbon. Although DBC is much more stable than natural peroxidases such as HRP, further research is needed to determine if this translates to a longer duration of such catalytic activity and effects. The structure-activity relationships for the peroxidase-like activity of DBC also need future investigation. Overall, the peroxidase-like activity of DBC discovered here has significant implications for the biogeochemical processing of organic carbon, including natural attenuation of pollutants, and the ecological impacts of black carbon. The present study also underscores the

important role of naturally occurring organic catalysts in environmental systems, which warrants systematic investigation.

CRediT authorship contribution statement

Yi Tan: Investigation, Methodology, Writing – original draft. **Su Sun:** Investigation. **Zehui Deng:** Methodology, Writing – review & editing. **Pedro J.J. Alvarez:** Methodology, Writing – review & editing. **Xiaolei Qu:** Conceptualization, Methodology, Supervision, Writing – review & editing.

Data availability

Data will be made available on request.

Declaration of competing interest

The authors declare that they have no known competing financial interests or personal relationships that could have appeared to influence the work reported in this paper.

Acknowledgements

This work was supported by the National Key Research and Development Program of China (2019YFC1804201 and 2020YFC1807002) and the NSF ERC, U.S.A on Nanotechnology-Enabled Water Treatment (EEC-1449500).

Appendix A. Supplementary data

Supplementary data to this article can be found online at https://doi.org/10.1016/j.scitotenv.2023.165347.

References

Aitipamula, S., Chow, P.S., Tan, R.B.H., 2011. Structural, spectroscopic and thermal analysis of cocrystals of carbamazepine and Piracetam with hydroquinone. J. Chem. Crystallogr. 41 (11), 1604–1611.

Bilal, M., Rasheed, T., Iqbal, H.M.N., Yan, Y.J., 2018. Peroxidases-assisted removal of environmentally-related hazardous pollutants with reference to the reaction mechanisms of industrial dyes. Sci. Total Environ. 644, 1–13.

Cançado, L.G., Takai, K., Enoki, T., Endo, M., Kim, Y.A., Mizusaki, H., Jorio, A., Coelho, L.N., Magalhães-Paniago, R., Pimenta, M.A., 2006. General equation for the determination of the crystallite size La of nanographite by Raman spectroscopy. Appl. Phys. Lett. 88 (16).

Chen, C.Y., Jafvert, C.T., 2011. The role of surface functionalization in the solar light-induced production of reactive oxygen species by single-walled carbon nanotubes in water. Carbon 49 (15), 5099–5106.

Chen, C., Fu, X., Fan, W., Ma, T., Wang, Z., Miao, S., 2015. In-situ synthesis of core/shell structured polypyrrole/hydroquinone nano-beads and electrochemical capacitance investigations. Mater. Lett. 138, 279–283.

Chen, M., Yang, B., Zhu, J., Liu, H., Zhang, X., Zheng, X., Liu, Q., 2018. FePt nanoparticles-decorated graphene oxide nanosheets as enhanced peroxidase mimics for sensitive response to H2O2. Mater. Sci. Eng. C 90, 610–620.

Du, Z., He, Y., Fan, J., Fu, H., Zheng, S., Xu, Z., Qu, X., Kong, A., Zhu, D., 2018. Predicting apparent singlet oxygen quantum yields of dissolved black carbon and humic substances using spectroscopic indices. Chemosphere 194, 405–413.

Fan, K., Xi, J., Fan, L., Wang, P., Zhu, C., Tang, Y., Xu, X., Liang, M., Jiang, B., Yan, X., Gao, L., 2018. In vivo guiding nitrogen-doped carbon nanozyme for tumor catalytic therapy. Nat. Commun. 9 (1), 1440.

Fang, G., Liu, C., Wang, Y., Dionysiou, D.D., Zhou, D., 2017. Photogeneration of reactive oxygen species from biochar suspension for diethyl phthalate degradation. Appl. Catal. B Environ. 214, 34–45.

Fu, H., Liu, H., Mao, J., Chu, W., Li, Q., Alvarez, P.J.J., Qu, X., Zhu, D., 2016. Photochemistry of dissolved black carbon released from biochar: reactive oxygen species generation and phototransformation. Environ. Sci. Technol. 50 (3), 1218–1226.

Fu, H., Wei, C., Qu, X., Li, H., Zhu, D., 2018a. Strong binding of apolar hydrophobic organic contaminants by dissolved black carbon released from biochar: a mechanism of pseudomicelle partition and environmental implications. Environ. Pollut. 232, 402–410.

Fu, H., Zhou, Z., Zheng, S., Xu, Z., Alvarez, P.J.J., Yin, D., Qu, X., Zhu, D., 2018b. Dissolved mineral ash generated by vegetation fire is photoactive under the solar spectrum. Environ. Sci. Technol. 52 (18), 10453–10461.

Gao, L., Zhuang, J., Nie, L., Zhang, J., Zhang, Y., Gu, N., Wang, T., Feng, J., Yang, D., Perrett, S., Yan, X., 2007. Intrinsic peroxidase-like activity of ferromagnetic nanoparticles. Nat. Nanotechnol. 2 (9), 577–583.

Goldstone, J.V., Pullin, M.J., Bertilsson, S., Voelker, B.M., 2002. Reactions of hydroxyl radical with humic substances: bleaching, mineralization, and production of bioavailable carbon substrates. Environ. Sci. Technol. 36 (3), 364–372.

Haag, W.R., Hoigne, J.R., Gassman, E., Braun, A.M., 1984. Singlet oxygen in surface waters — part I: furfuryl alcohol as a trapping agent. Chemosphere 13 (5), 631–640.

Han, L., Li, C., Zhang, T., Lang, Q., Liu, A., 2015. Au@Ag heterogeneous nanorods as nanozyme interfaces with peroxidase-like activity and their application for one-pot analysis of glucose at nearly neutral pH. ACS Appl. Mater. Interfaces 7 (26), 14463–14470.

Ishibashi, K.-I., Fujishima, A., Watanabe, T., Hashimoto, K., 2000. Detection of active oxidative species in TiO2 photocatalysis using the fluorescence technique. Electrochem. Commun. 2 (3), 207–210.

Jaffe, R., Ding, Y., Niggemann, J., Vahatalo, A.V., Stubbins, A., Spencer, R.G.M., Campbell, J., Dittmar, T., 2013. Global charcoal mobilization from soils via dissolution and riverine transport to the oceans. Science 340 (6130), 345–347.

Jian, T., Zhou, Y., Wang, P., Yang, W., Mu, P., Zhang, X., Zhang, X., Chen, C.-L., 2022. Highly stable and tunable peptoid/hemin enzymatic mimetics with natural peroxidase-like activities. Nat. Commun. 13 (1), 3025.

Li, R., Zhen, M., Guan, M., Chen, D., Zhang, G., Ge, J., Gong, P., Wang, C., Shu, C., 2013. A novel glucose colorimetric sensor based on intrinsic peroxidase-like activity of C60-carboxyfullerenes. Biosens. Bioelectron. 47, 502–507.

Lian, F., Yu, W., Zhou, Q., Gu, S., Wang, Z., Xing, B., 2020. Size matters: nano-biochar triggers decomposition and transformation inhibition of antibiotic resistance genes in aqueous environments. Environ. Sci. Technol. 54 (14), 8821–8829.

Lian, F., Zhang, Y., Gu, S., Han, Y., Cao, X., Wang, Z., Xing, B., 2021. Photochemical transformation and catalytic activity of dissolved black nitrogen released from environmental black carbon. Environ. Sci. Technol. 55 (9), 6476–6484.

Liu, Y., Luo, J., Tang, L., Feng, C., Wang, J., Deng, Y., Liu, H., Yu, J., Feng, H., Wang, J., 2020. Origin of the enhanced reusability and electron transfer of the carbon-coated Mn3O4 nanocube for persulfate activation. ACS Catal. 10 (24), 14857–14870.

Lou, Z., Zhao, S., Wang, Q., Wei, H., 2019. N-doped carbon as peroxidase-like nanozymes for total antioxidant capacity assay. Anal. Chem. 91 (23), 15267–15274.

Ma, J., Del Vecchio, R., Golanoski, K.S., Boyle, E.S., Blough, N.V., 2010. Optical properties of humic substances and CDOM: effects of borohydride reduction. Environ. Sci. Technol. 44 (14), 5395–5402.

Marinoni, A., Parazols, M., Brigante, M., Deguillaume, L., Amato, P., Delort, A.-M., Laj, P., Mailhot, G., 2011. Hydrogen peroxide in natural cloud water: sources and photoreactivity. Atmos. Res. 101 (1), 256–263.

Masiello, C.A., 2004. New directions in black carbon organic geochemistry. Mar. Chem. 92 (1–4), 201–213.

McKay, G., Couch, K.D., Mezyk, S.P., Rosario-Ortiz, F.L., 2016. Investigation of the coupled effects of molecular weight and charge-transfer interactions on the optical and photochemical properties of dissolved organic matter. Environ. Sci. Technol. 50 (15), 8093–8102.

Ndungu, L.K., Steele, J.H., Hancock, T.L., Bartleson, R.D., Milbrandt, E.C., Parsons, M.L., Urakawa, H., 2019. Hydrogen peroxide measurements in subtropical aquatic systems and their implications for cyanobacterial blooms. Ecol. Eng. 138, 444–453.

Page, S.E., Arnold, W.A., McNeill, K., 2010. Terephthalate as a probe for photochemically generated hydroxyl radical. J. Environ. Monit. 12 (9), 1658–1665.

Page, S.E., Sander, M., Arnold, W.A., McNeill, K., 2012. Hydroxyl radical formation upon oxidation of reduced humic acids by oxygen in the dark. Environ. Sci. Technol. 46 (3), 1590–1597.

Qu, X., Fu, H., Mao, J., Ran, Y., Zhang, D., Zhu, D., 2016. Chemical and structural properties of dissolved black carbon released from biochars. Carbon 96, 759–767.

Shaked, Y., Harris, R., Klein-Kedem, N., 2010. Hydrogen peroxide photocycling in the Gulf of Aqaba, Red Sea. Environ. Sci. Technol. 44 (9), 3238–3244.

Sharpless, C.M., 2012. Lifetimes of triplet dissolved natural organic matter (DOM) and the effect of NaBH4 reduction on singlet oxygen quantum yields: implications for DOM photophysics. Environ. Sci. Technol. 46 (8), 4466–4473.

Shi, W., Wang, Q., Long, Y., Cheng, Z., Chen, S., Zheng, H., Huang, Y., 2011. Carbon nanodots as peroxidase mimetics and their applications to glucose detection. Chem. Commun. 47 (23), 6695–6697.

Song, Y., Qu, K., Zhao, C., Ren, J., Qu, X., 2010a. Graphene oxide: intrinsic peroxidase catalytic activity and its application to glucose detection. Adv. Mater. 22 (19), 2206–2210.

Song, Y., Wang, X., Zhao, C., Qu, K., Ren, J., Qu, X., 2010b. Label-free colorimetric detection of single nucleotide polymorphism by using single-walled carbon nanotube intrinsic peroxidase-like activity. Chem. Eur. J. 16 (12), 3617–3621.

Song, F., Li, T., Shi, Q., Guo, F., Bai, Y., Wu, F., Xing, B., 2021. Novel insights into the molecular-level mechanism linking the chemical diversity and copper binding heterogeneity of biochar-derived dissolved black carbon and dissolved organic matter. Environ. Sci. Technol. 55 (17), 11624–11636.

Sun, H., Gao, N., Dong, K., Ren, J., Qu, X., 2014. Graphene quantum dots-band-aids used for wound disinfection. ACS Nano 8 (6), 6202–6210.

Sun, H., Zhao, A., Gao, N., Li, K., Ren, J., Qu, X., 2015. Deciphering a nanocarbon-based artificial peroxidase: chemical identification of the catalytically active and substrate-binding sites on graphene quantum dots. Angew. Chem. Int. Ed. 54 (24), 7176–7180.

Sutherland, M.W., Learmonth, B.A., 1997. The tetrazolium dyes MTS and XTT provide new quantitative assays for superoxide and superoxide dismutase. Free Radic. Res. 27 (3), 283–289.

Tinnacher, R.M., Honeyman, B.D., 2007. A new method to radiolabel natural organic matter by chemical reduction with tritiated sodium borohydride. Environ. Sci. Technol. 41 (19), 6776–6782.

Wan, D., Wang, J., Dionysiou, D.D., Kong, Y., Yao, W., Selvinsimpson, S., Chen, Y., 2021. Photogeneration of reactive species from biochar-derived dissolved black carbon for the degradation of amine and phenolic pollutants. Environ. Sci. Technol. 55 (13), 8866–8876.

Wang, X., Qu, K., Xu, B., Ren, J., Qu, X., 2011. Multicolor luminescent carbon nanoparticles: synthesis, supramolecular assembly with porphyrin, intrinsic peroxidase-like catalytic activity and applications. Nano Res. 4, 908–920.

Wang, D., Song, X., Li, P., Gao, X.J., Gao, X., 2020a. Origins of the peroxidase mimicking activities of graphene oxide from first principles. J. Mater. Chem. B 8 (39), 9028–9034.

Wang, H., Zhou, H., Ma, J., Nie, J., Yan, S., Song, W., 2020b. Triplet photochemistry of dissolved black carbon and its effects on the photochemical formation of reactive oxygen species. Environ. Sci. Technol. 54 (8), 4903–4911.

Wang, H., Han, M., Wang, M., Zhou, H., 2022. Microheterogeneous triplet oxidation of hydrophobic organic contaminants in dissolved black carbon solutions under simulated solar irradiation. Environ. Sci. Technol. 56 (20), 14574–14584.

Wilkinson, K.J., Balnois, E., Leppard, G.G., Buffle, J., 1999. Characteristic features of the major components of freshwater colloidal organic matter revealed by transmission electron and atomic force microscopy. Colloids Surf. A Physicochem. Eng. Asp. 155 (2), 287–310.

Wilson, C.L., Hinman, N.W., Cooper, W.J., Brown, C.F., 2000. Hydrogen peroxide cycling in surface geothermal waters of Yellowstone National Park. Environ. Sci. Technol. 34 (13), 2655–2662.

Woolf, D., Amonette, J.E., Street-Perrott, F.A., Lehmann, J., Joseph, S., 2010. Sustainable biochar to mitigate global climate change. Nat. Commun. 1, 9.

Xu, F., Wei, C., Zeng, Q., Li, X., Alvarez, P.J.J., Li, Q., Qu, X., Zhu, D., 2017. Aggregation behavior of dissolved black carbon: implications for vertical mass flux and fractionation in aquatic systems. Environ. Sci. Technol. 51 (23), 13723–13732.

Yuan, J., Shiller, A.M., 2000. The variation of hydrogen peroxide in rainwater over the south and Central Atlantic Ocean. Atmos. Environ. 34 (23), 3973–3980.

Yuan, X., Nico, P.S., Huang, X., Liu, T., Ulrich, C., Williams, K.H., Davis, J.A., 2017. Production of hydrogen peroxide in groundwater at rifle, Colorado. Environ. Sci. Technol. 51 (14), 7881–7891.

Zhao, R., Zhao, X., Gao, X., 2015. Molecular-level insights into intrinsic peroxidase-like activity of nanocarbon oxides. Chem. Eur. J. 21 (3), 960–964.

Zheng, A.-X., Cong, Z.-X., Wang, J.-R., Li, J., Yang, H.-H., Chen, G.-N., 2013. Highly-efficient peroxidase-like catalytic activity of graphene dots for biosensing. Biosens. Bioelectron. 49, 519–524.

Zhou, Z., Chen, B., Qu, X., Fu, H., Zhu, D., 2018. Dissolved black carbon as an efficient sensitizer in the photochemical transformation of 17β-estradiol in aqueous solution. Environ. Sci. Technol. 52 (18), 10391–10399.